Ultrafast laser-induced refractive index tuning inside GeSbSNa glasses for mid-IR applications

Research Article Vol. 34, No. 3 / 9 Feb 2026 / Optics Express 4535
Optics EXPRESS

Ultrafast laser-induced refractive index tuning inside GeSbSNa glasses for mid-IR applications

HENG YAO,[1,2] JULIEN ARI,[2] DIEGO PUGLIESE,[3] MARC DUSSAUZE,[4] JIANRONG QIU,[1,5,6] AND MATTHIEU LANCRY[2,7]

[1]*Institute of Light+X Science and Technology, College of Information Science and Engineering, Ningbo University, Ningbo 315211, China*
[2]*Institut de Chimie Moléculaire et des Matériaux d'Orsay, CNRS, Université Paris-Saclay, Orsay 91400, France*
[3]*Division of Applied Metrology and Engineering, National Institute of Metrological Research (INRiM), Turin 10135, Italy*
[4]*Institut des Sciences Moléculaires, UMR 5255, Université de Bordeaux, Talence Cedex 33405, France*
[5]*College of Optical Science and Engineering, Zhejiang University, Hangzhou 310027, China*
[6]*qjr@zju.edu.cn*
[7]*matthieu.lancry@universite-paris-saclay.fr*

Abstract: Femtosecond laser direct writing (FLDW) enables precise, three-dimensional (3D) structuring within transparent materials, offering a versatile platform for integrated photonics. In this work, we investigate the photo-response of sodium-doped GeSbS (GeSbSNa) chalcogenide glasses under femtosecond laser irradiation, a system of interest for mid-infrared (MIR) applications yet largely unexplored. Through quantitative phase microscopy, we extract refractive index changes as a function of composition and laser pulse energy, achieving phase shifts up to 62 radians and refractive index contrasts (Δn) exceeding 0.05—among the highest reported for chalcogenide systems. Raman spectroscopy reveals localized structural reorganizations, notably a transition from corner- to edge-sharing GeS_4 tetrahedra, consistent with laser-induced densification. We also evaluate the thermal stability of the modifications via isochronal annealing and compare them with commercial glass benchmarks. Overall, these results provide a quantitative basis for assessing GeSbSNa glasses as prospective materials for MIR photonic integration, particularly in contexts where both high photosensitivity and moderate thermal durability are desirable, even though no specific devices are demonstrated here.

1. Introduction

Femtosecond (fs) laser direct writing (FLDW) has emerged as a transformative tool for the fabrication of compact, three-dimensional (3D) photonic structures within transparent materials [1–5]. By leveraging ultrashort laser pulses, FLDW enables localized and permanent modifications in bulk media through nonlinear optical ionization, reaching extreme energy densities on the order of terawatts per square centimeters [6]. This capability offers unprecedented control over material structuring at the microscale, facilitating the creation of waveguides, gratings, and lenses directly embedded within optical substrates [7–9]. Consequently, applications such as in-line holography using a unified compressive phase retrieval framework [10], multiplexed optical data storage or birefringence patterning [11], and the realization of low-loss waveguides or fiber Bragg gratings in the mid-infrared (MIR) [12–14], become accessible.

Among the materials suitable for FLDW, chalcogenide glasses (ChGs) have attracted significant interest due to their unique combination of properties: a wide infrared (IR) transmission window

#583039 https://doi.org/10.1364/OE.583039
Journal © 2026 Received 30 Oct 2025; revised 18 Jan 2026; accepted 19 Jan 2026; published 30 Jan 2026

Optics EXPRESS

(up to ~28 μm), high Kerr nonlinearity, large refractive index, and pronounced photosensitivity [15,16] compared to oxide glasses, like heavy metal oxide [5] or SiO_2 glasses [15,17]. These attributes render ChGs ideal for MIR integrated photonics, particularly in fields such as stimulated Brillouin scattering [18], chemical sensing [19], waveguides [20], nonlinear optics, and broadband supercontinuum generation [21].

Ge–Sb–S-based chalcogenide glasses, in particular, stand out due to their broad transmission window (0.5–10 μm), strong optical nonlinearity, and low thermo-refractive coefficient, making them superior candidates for MIR photonic devices compared to conventional oxide glasses. Despite growing interest, the response of these glasses—especially when doped with network modifiers such as sodium—under fs laser irradiation remains poorly understood.

This study investigates fs laser-induced modifications in sodium-doped GeSbS (GeSbSNa) glasses, a system not previously explored in this context. We systematically assess the impact of composition and laser parameters on refractive index changes, phase shifts, and thermal stability. By combining quantitative phase microscopy and Raman spectroscopy, we link optical modifications to underlying structural transformations, providing insights into the tunability and resilience of GeSbSNa glasses for MIR photonic integration.

2. Experimental section

2.1. Glass synthesis and characterization

Chalcogenide glasses (ChGs) were prepared using high-purity elemental Ge, Sb, and S (Alfa Aesar, 99.999%). Anhydrous sodium sulfide was employed as a sodium dopant. Based on the stoichiometric composition $Ge_{25}Sb_{10}S_{65}$, various samples were synthesized either by varying the S/Ge ratio (i.e., increasing the sulfur content) or by keeping this ratio constant while introducing sodium. The nominal compositions of the different glasses, along with their corresponding labels, are listed in Table 1. Two series of glasses were synthesized as follows: (i) Samples A, B, and D with a fixed sodium content to investigate the effect of sulfur concentration, and (ii) Samples Na0, Na0.5, Na1, Na2, and Na5.5 with a constant S/Ge ratio to explore the influence of sodium content. All samples were prepared as double-side polished slices with a thickness of (2.0 ± 0.1) mm.

Table 1. Label and batch composition of the GeSbSNa glasses used in this work, along with the composition ratios

		Composition (at.%)				
	Sample	Ge	Sb	S	Na	S/Ge ratio
S/Ge ratio effect	A	24.5	10	64.5	1	2.6
	B	22	10	67	1	3
	D	17	10	72	1	4.2
Na content effect	Na0	22.5	10	67.5	0	3
	Na0.5	22.4	10	67.1	0.5	3
	Na1	22	10	67	1	3
	Na2	22	9.8	66.2	2	3
	Na5.5	21.3	9.4	64.8	5.5	3

The raw materials were weighed in a glovebox under a nitrogen atmosphere and then loaded into a quartz ampoule, which was evacuated to 10^{-2} mbar and sealed using an oxygen-methane torch. A rocking furnace was used during the melting process to ensure homogeneous mixing. The temperature was raised at a rate of 1 °C/min up to 850 °C and held for 12 h for homogenization. The rocking motion was then stopped, and the temperature gradually decreased to 750 °C for quenching. The melt was quenched in water and annealed for 6 h at 10 °C below the glass transition temperature (T_g). T_g was measured using differential scanning calorimetry (DSC) and

Optics EXPRESS

differential thermal analysis (DTA) with a Netzsch Pegasus 404 apparatus. Glass chunks were placed in a platinum pan and heated at a rate of 10 °C/min, with a measurement precision of ±2 °C. The T_g values for the different glasses ranged between 250 and 350 °C [19].

Raman spectra were collected using an XploRA PLUS (Horiba) spectrometer equipped with a 785 nm excitation laser, focused on the sample surface using a 50× objective lens. Raman mapping was performed over an 80 × 60 μm^2 area using a high-resolution 100× objective lens (numerical aperture NA = 0.9), achieving a lateral spatial resolution of approximately 2 μm during the scan.

Besides, optical transmission measurements were performed at room temperature for each glass composition over the UV-Visible-NIR and MIR spectral ranges, using an Agilent Cary 5000 and a Bruker Equinox 55 spectrophotometer, respectively. Figure 1 shows the linear transmission spectrum of the GeSbSNa-ANa0.5 glass as a representative example. The spectrum confirms a broad transparency window extending from the visible to the MIR region, with no detectable absorption bands around 750 nm. A weak absorption feature is observed near 4000 nm, which is attributed to S–H vibrational bonds. Similar transmission spectra were measured for all other GeSbSNa compositions and showed comparable transparency windows, with no absorption bands around 750 nm.

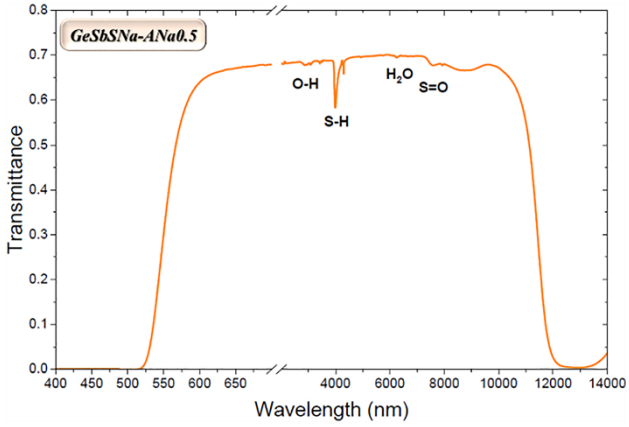

Fig. 1. Linear transmission spectrum of GeSbSNa-ANa0.5 glass as a function of wavelength.

2.2. *Fs laser irradiation and characterization of laser-written modified regions*

Each sample was double-side polished to optical quality prior to fs laser irradiation using a Satsuma laser system (Amplitude Systèmes Ltd., Pessac, France). The laser operated at a central wavelength of 1030 nm with a repetition rate of 100 kHz, pulse duration of 800 fs, and writing speed of 1 mm/s, corresponding to a pulse density of 100 pulses/μm. Linearly polarized light was used, with polarization aligned along the x-axis (defined by the laser compressor plane). The beam was focused 300 μm below the surface (in air) using a 0.6 NA aspheric lens with a 4 mm focal length. Pulse energy ranged from 0.001 to 1 μJ. For all compositions and pulse energies investigated in this work, rectangular patterns were written using a horizontal scanning motion with a 1 μm pitch, combining displacements along two axes via a high precision xyz stage. Each rectangle owns lateral dimensions of approximately 10 × 100 μm^2 and is written at a depth of 300 μm below the sample surface. A spiral-disk geometry with a 1 μm pitch is also used for representative graded-index structures, where the pulse energy is intentionally varied along the trajectory to generate a spatially graded refractive index profile.

Optics EXPRESS

Post-irradiation, isochronal annealing (carried out inside a furnace) was performed in 30-min steps by progressively increasing the temperature from room temperature up to $\sim 1.2 \times T_g$. The structures used for the thermal annealing experiments were Type I rectangular-like features written using the same geometry described above, at pulse energies corresponding to the plateau region for each composition (typically in the range 0.1–0.15 μJ). After each annealing step, the remaining phase shift $\Delta\phi(T)$ was measured and normalized to the initial phase shift $\Delta\phi_0$ measured at room temperature. The "90% erasure" temperature is defined as the temperature at which the normalized phase shift decreases to 10% of its initial value, i.e., $\Delta\phi(T)/\Delta\phi_0 = 0.10$. For each glass composition, this value was obtained by averaging the measurements over at least three nominally identical structures written under the same conditions. Optical characterization after each annealing step was conducted using an Olympus BX51 microscope in transmission mode under natural light. In addition to conventional optical microscopy, quantitative phase microscopy (QPM, Iatia) was employed to measure the optical phase shift ($\Delta\phi$, in radians (rad)) induced by the irradiated structures relative to the pristine glass. All reported phase shifts were measured at or near the center of the written features, where $\Delta\phi$ is maximal. The corresponding refractive index change (RIC) was calculated using the relation: $\Delta n = \Delta\phi\lambda / 2\pi d$, where $\lambda = 750$ nm is the illumination wavelength used in QPM, and d is the geometric thickness of the laser-modified region. The uncertainty in Δn mainly arises from the uncertainty in the retrieved phase shift $\Delta\phi$ and from the uncertainty in the geometric thickness d of the modified region. The phase uncertainty obtained from QPM is typically up to ±3 rad for the highest phase values, while the uncertainty on d, estimated from repeated measurements on calibrated cross-sectional images, is about ±2 μm for modified regions with thicknesses ranging from 50 to 200 μm. By propagation of these uncertainties, the resulting relative uncertainty on Δn is estimated to remain below approximately 6–9%.

The geometric thickness d of the laser-modified region was extracted from calibrated cross-sectional optical microscopy images acquired on representative laser tracks using a high-magnification objective. For each structure, d is defined as the extent of the region along the laser propagation direction where the optical/QPM contrast significantly differs from the pristine background. The RIC is not expected to be strictly uniform along the axial direction; instead, it is typically peaked around the focal region and gradually decays away from it. Therefore, the use of a single thickness d in $\Delta n = \Delta\phi\lambda/2\pi d$ corresponds to an effective uniform-slab approximation that reproduces the measured integrated phase shift "seen along the light propagation". Accordingly, Δn should be interpreted as an effective average RIC over the modified thickness, rather than a local peak value. A full 3D reconstruction of Δn (x,y,z) would require phase tomography and is beyond the scope of the present work.

The choice of the 750 nm probe wavelength is motivated by both instrumental and material considerations. From an instrumental standpoint, the QPM system operates optimally in the red/near-IR region (700–800 nm), offering a good compromise between spatial resolution and detector sensitivity. From a material perspective, as confirmed by the transmission spectrum presented in Fig. 1, the GeSbSNa compositions examined in this study exhibit negligible absorption around 750 nm. Therefore, the measured phase shift is dominated by changes in the real part of the refractive index and is not affected by absorption-related artifacts.

3. Results and discussion

Figure 2 presents the range of structural modifications induced by fs laser irradiation in various GeSbSNa glasses. The observed regimes include: no modification, Type I, bubbles formation, spatial broadening regime + bubbles, and spatial broadening regime only. These regimes are denoted by distinct symbols as shown in the figure legend. Due to the high optical nonlinearity of chalcogenide glasses and the use of a high repetition rate, nonlinear propagation effects such

Optics EXPRESS

as self-focusing and filamentation may occur at elevated pulse energies, leading to extended modified regions and contributing to the transition between these different modification regimes.

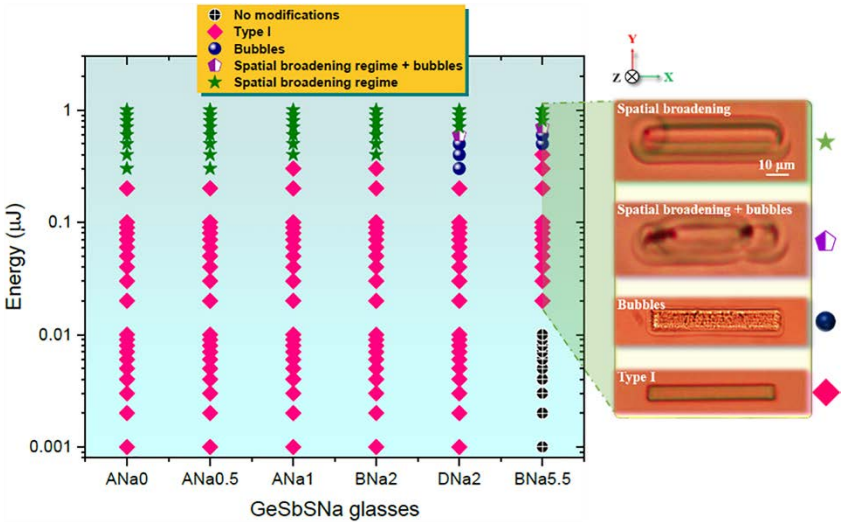

Fig. 2. Left: laser-induced modification regimes in GeSbSNa glasses as a function of pulse energy. Distinct structural responses are identified: no modification (black cross), Type I (pink diamond), bubble formation (blue circle), spatial broadening with bubbles (purple circle), and spatial broadening only (green star). The data highlight the influence of glass composition on the energy thresholds for modification, with sodium-rich glasses exhibiting slightly elevated thresholds. Right: optical microscope image of 4 different types of laser-induced modifications, with Z being laser propagation direction. All samples were irradiated using fs laser pulses (1030 nm, 800 fs, 100 kHz) with a writing speed of 1 mm/s.

Generally, the threshold for Type I modification [22] is slightly influenced by the chemical composition of the glass and sometimes attributed to structural relaxation followed by a fast quenching [5]. In this study, the deviation in the Type I formation threshold between GeSbSNa-BNa5.5 (~0.02 μJ) and the other compositions (~0.001 μJ) remains within one order of magnitude. This suggests a slightly increased energy requirement for inducing modifications in glasses with higher alkali content [23, 24], as illustrated in Fig. 2. The energy window for Type I modifications spans approximately from 0.001 to 0.2 μJ across all compositions.

Interestingly, GeSbSNa-DNa2 and GeSbSNa-BNa5.5 glasses exhibit the formation of bubbles and the spatial broadening regime + bubbles in the intermediate energy ranges of 0.3–0.6 μJ and 0.5–0.7 μJ, respectively. These features tend to occur in glasses with higher concentrations of network modifiers (e.g., Na^+) and lower proportions of network formers (e.g., Ge). Here, "network formers" (e.g., Ge and Sb) refer to elements that build the covalent backbone of the glass through polyhedral units (e.g., GeS_4 tetrahedra and SbS_3 pyramids), whereas "network modifiers" (e.g., Na^+) do not belong to the continuous covalent network and instead occupy interstitial sites and/or disrupt network connectivity, thereby altering local field strength, density, refractive index, and T_g.

At higher pulse energies or under high repetition rates, another regime—referred to as the spatial broadening regime—emerges, represented by green asterisks in Fig. 2. This regime is characterized by a Type I-like morphology (but the modified zone becomes significantly elongated in all directions and the width is much beyond the optical beam size (due to heat accumulation) compared to the low energy Type I regime), and results from a pulse-to-pulse cumulative heat deposition. It is of particular interest for integrated photonic applications (e.g., waveguides) due

Optics EXPRESS

to its capability to induce significant phase shifts and refractive index changes [5]. Among all studied compositions, GeSbSNa-BNa5.5 consistently shows slightly elevated energy thresholds for all types of laser-induced modifications. This behavior might be attributed to the effect of alkali cations, acting as network modifiers that alter the glass structure and its laser sensitivity [25].

The photosensitivity of transparent glasses at the laser wavelength enables the induction of a localized phase shift through FLDW. In previous studies, high phase shifts—typically in the range of 6–8 rad—have been reported for Type I modifications in heavy metal oxide glasses, such as barium gallo-germanate (BGG), under similar fs laser exposure conditions [5]. Additionally, Lepicard et al. [26] demonstrated phase shift generation via micro-scale thermoelectrical imprinting in GeSbSNa glasses, where the sodium content was shown to significantly influence surface topology, density contraction, and volume displacement, all contributing to local refractive index changes. The addition of sodium to the parent GeSbS glass can lead to an increase in the refractive index (e.g., from 2.181 to 2.207), resulting from changes in local density caused by the departure of Na^+ ions to maintain charge neutrality [26]. More recently, Yang et al. [27,28] reported the fabrication of gradient refractive index microlens arrays in chalcohalide glasses using microthermal poling, achieving phase shifts ranging from approximately 2.2 to 7.5 rad under monochromatic illumination ($\lambda = 632.8$ nm). These results highlight the critical role of glass composition and processing method in controlling refractive index modulation.

In this context, Fig. 3 presents the evolution of phase shift and geometric thickness of the modified region as a function of laser pulse energy for several GeSbSNa glass compositions. Panel (a) includes the ANa series with constant S/Ge ratio (2.6) and varying sodium content (Na0, Na0.5, Na1), while panel (b) displays the BNa and DNa series with fixed sodium content but different S/Ge ratios (3 and 4.2, respectively).

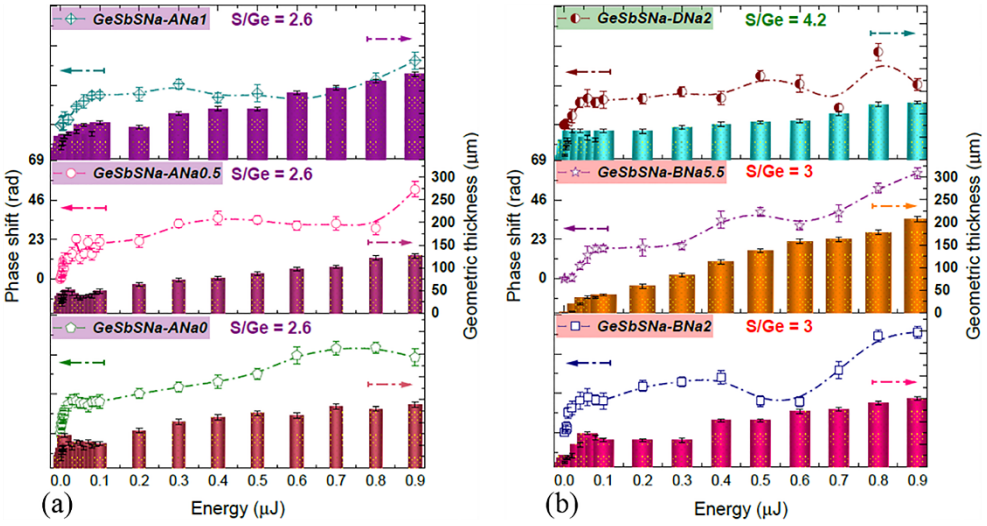

Fig. 3. Phase shift (symbols and dashed lines, left axis) and geometric thickness of the laser-modified region (bars, right axis) as a function of laser pulse energy for different GeSbSNa compositions. (a) Sodium variation at constant S/Ge ratio (S/Ge = 2.6; Na0, Na0.5, and Na1). (b) Series with varying S/Ge ratios (S/Ge = 4.2, 3, 3). The plotted phase shifts correspond to the average $\Delta\phi$ measured at the center of each structure. Lines are guides to the eye only. Error bars represent one standard deviation of the measurements within the analyzed region.

Optics EXPRESS

In general, the phase shift increases with pulse energy, exhibiting a steep rise around 0.09 μJ, followed by a more gradual increase at higher energies. Phase shift values span from approximately 23 rad (plateau region) to 62 rad (maximum), which corresponds to relatively high refractive index changes, competitive with values reported in the literature for similar glass systems [5,27,28].

The geometric thickness of the modified region also increases with pulse energy, indicating the volumetric growth of the laser-affected zone. The cross-sectional image reveals structures that extend over several tens of micrometers along the laser propagation direction, consistent with the formation dynamics of Type I modifications [29]. Importantly, above a critical pulse energy (~0.2 μJ in GeSbSNa), a secondary non-diverging trace appears beyond the main modification, and it marks the onset of more complex propagation regimes beyond the linear focus [30]. This effect is attributed to filamentation, resulting from a balance between self-focusing due to nonlinear refractive index (n_2) increase and defocusing caused by free-electron plasma formation. These observations highlight the strong dependence of fs laser interaction dynamics on both composition (Na content, S/Ge ratio) and energy regime, confirming that controlled tuning of these parameters is essential for precise and repeatable refractive index modification in chalcogenide-based photonic materials.

The RIC, Δn, was calculated using the relation $\Delta n = \Delta\phi\lambda \,/\, 2\pi d$, where $\Delta\phi$ is the measured phase shift (in rad), λ is the probe wavelength (750 nm), and d is the geometric thickness of the modified region [5]. Figure 4 presents both the maximum and mean RICs as a function of the S/Ge ratio in the GeSbSNa glass series. For each glass composition, the mean RIC corresponds to the representative plateau phase shift measured at intermediate pulse energies (typically around 0.1 μJ), while the maximum RIC is extracted from the highest phase shift values obtained at higher pulse energies, as shown in Fig. 3. In Fig. 3, all plotted phase shift values correspond to the maximum $\Delta\phi$ measured at or near the center of each written structure. A clear decreasing trend is observed: the maximum Δn drops from approximately 0.05 in GeSbSNa-ANa0.5 to about 0.032 in GeSbSNa-DNa2. Nevertheless, these values remain significantly higher than those typically reported in oxide-based glasses such as barium gallo-germanate (BGG) under comparable fs laser writing conditions, for which maximum RICs in the range $\Delta n \approx 0.01$–0.015 are reported [5]. This corresponds to a factor of about 3–5 lower than the maximum values achieved in the present GeSbSNa glasses.

Although the RIC was directly measured at 750 nm using QPM, the laser-induced modifications reported here are densification-driven and occur well within the transparency window of the glass. Under such conditions, the relative RIC is expected to be only weakly dispersive across the visible–MIR spectral range and primarily governed by local density and polarizability changes rather than by resonant absorption (e.g. point defects). Within a Lorentz–Lorenz or Sellmeier-type framework, a given change in local density leads to a fractional RIC that remains of the same order of magnitude at longer wavelengths. Therefore, Δn values in the MIR (2–5 μm) are expected to be comparable, though possibly slightly smaller in absolute value, than those measured at 750 nm. A direct wavelength-dependent characterization of Δn in the MIR will nevertheless be an important perspective of future work.

This pronounced refractive index tunability is indicative of reduced glass connectivity with increasing sulfur content, a trend previously explained by a combination of hydrodynamic expansion and thermomechanical relaxation following laser exposure [31]. Furthermore, Raman spectroscopy has revealed that as the sulfur content increases, new vibrational bands emerge (e.g., at 152, 219, and 474 cm^{-1}), corresponding to homopolar S–S bonds [19]. At high S/Ge ratios, the formation of sulfur rings (S_8) by fs laser may become thermodynamically favorable structures known to be the most stable and abundant [32].

Another contributing factor to the observed trend is the progressive dilution of germanium—a strong network former—as the S/Ge ratio increases. A reduced Ge content weakens the structural

Optics EXPRESS

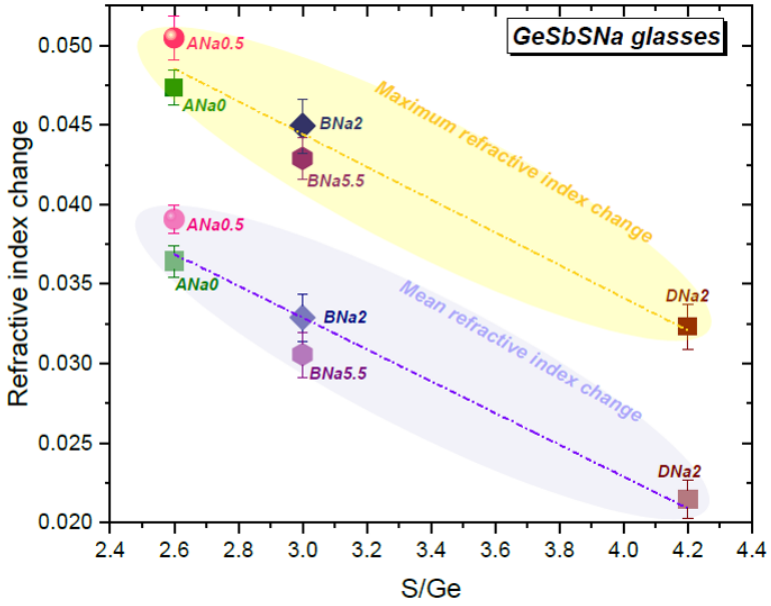

Fig. 4. Maximum and mean refractive index changes (Δn) as a function of the S/Ge ratio in GeSbSNa glasses. For each composition, the maximum Δn corresponds to the highest value according to pulse energy, while the mean Δn corresponds to the typical Δn measured at "the plateau" (see Fig. 3). A decreasing trend is observed with increasing sulfur content, indicating reduced glass connectivity and densification efficiency under fs laser exposure. Colored ellipses highlight the trend for maximum (yellow) and mean (purple) Δn values across the sodium-doped series. Error bars denote standard deviation of Δn considering phase and geometric thickness error bars.

backbone of the glass, while promoting sulfur-rich tetrahedral units (e.g., GeS_{4-x}), which may stabilize excess free sulfur and contribute to less pronounced laser-induced densification [33].

Finally, the mean RICs, which offer a more reliable metric from an engineering standpoint, follow the same decreasing trend. On average, the mean Δn values are about 20% lower than the corresponding maximum values, reflecting the spatial averaging of localized modifications and offering insight into the reproducibility and uniformity of the fs-induced transformations.

Figure 5 illustrates the quantitative phase analysis of a fs laser-written structure in GeSbSNa glass, i.e., a graded-index-like lens structure so called GRIN lens. Compared to traditional counterparts, the GRIN dispersive objective lens offers significant advantages, including a more compact design, a smaller diameter, and greatly enhanced measurement range and resolution. As a result, it enables more precise and easier measurement in practical scenarios [34]. The spatial phase distribution, shown in Fig. 5(a), reveals a symmetric circular pattern centered on the laser-modified region, corresponding to a spiral scan with 1 μm pitch (inset). A maximum phase shift is observed near the center of the structure, reaching values up to ~20 rad. During the inscription of the spiral-shaped graded-index structure, the pulse energy was intentionally varied from the center towards the periphery (from 0 up to ~0.4 μJ) in order to generate a parabolic dose distribution and mimic a GRIN lens profile. The radial phase gradient therefore directly reflects the accumulated local laser dose and underlies the focusing behavior of the structure. At the periphery of the graded index profile, a slight negative phase shift relative to the pristine glass is observed. This is attributed to the tensile stress field surrounding the densified core, which induces a stress-related region showing an opposite index change (elastic response) rather than a transition to a different damage regime. The fine radial bands visible in the phase image arise

Optics EXPRESS

from the discretization of the spiral trajectory into finite segments during writing, combined with small speed fluctuations between segments.

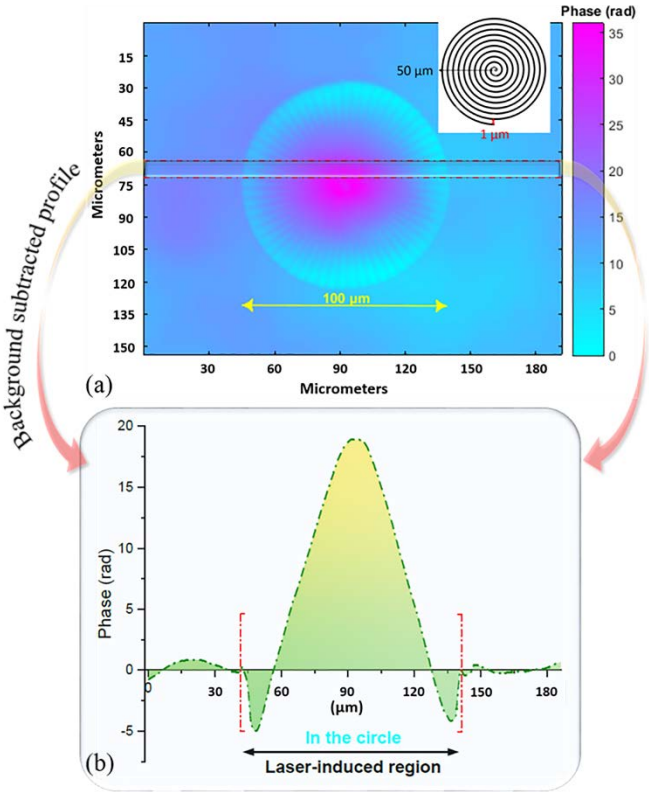

Fig. 5. (a) Quantitative phase image of a fs laser-written graded-index lens in GeSbSNa-ANa0 glass, showing a symmetric, circular phase distribution. Inset: spiral scanning pattern used for writing, pitch 1 µm. (b) Averaged horizontal phase profile along the dashed line in (a), revealing a peak phase shift of ~20 rad and a total diameter of about 100 µm. Superimposed small oscillations in the phase map correspond to the radial bands induced by the discretization of the spiral trajectory into finite segments during writing.

The horizontal phase profile (Fig. 5(b))—extracted along the dashed line and after baseline subtraction—confirms a smooth and localized graded-index distribution of the induced optical phase change. The laser-modified region is clearly bounded, as shown by the sharp phase drop (~-5 rad) at the edges, and spans approximately 100 µm in diameter. This high phase contrast is indicative of a substantial RIC at the center accompanied by a surrounding negative change, in agreement with the characteristics of the tensile stress field that necessarily develops in and around the laser irradiated zone. Such quantitative phase information provides direct insight into the extent of the structural and optical modifications and supports the potential of fs laser writing for high-contrast, localized photonic microstructuring in chalcogenide glasses e.g. to develop broadband and low-dispersion 3D integrated optics [1].

The thermal stability of laser-induced modifications is a critical parameter for real-world applications, especially in devices exposed to elevated temperatures such as optical sensors and integrated components in harsh environments. To evaluate this property for GeSbSNa glasses, the 90% erasure temperature of the laser-induced phase shift is plotted as a function of the glass transition temperature (T_g) in Fig. 6. For each glass composition, the remaining phase shift $\Delta\phi(T)$ of the test structures was measured after every 30-min annealing step and normalized to the

Optics EXPRESS

initial phase shift $\Delta\phi_0$ (20 °C) at room temperature. The "90 % erasure" temperature is defined here as the temperature at which $\Delta\phi(T)/\Delta\phi_0$ (20 °C) = 0.10. This erasure temperature serves as a key metric to assess the thermal durability of Type I modifications in transparent materials.

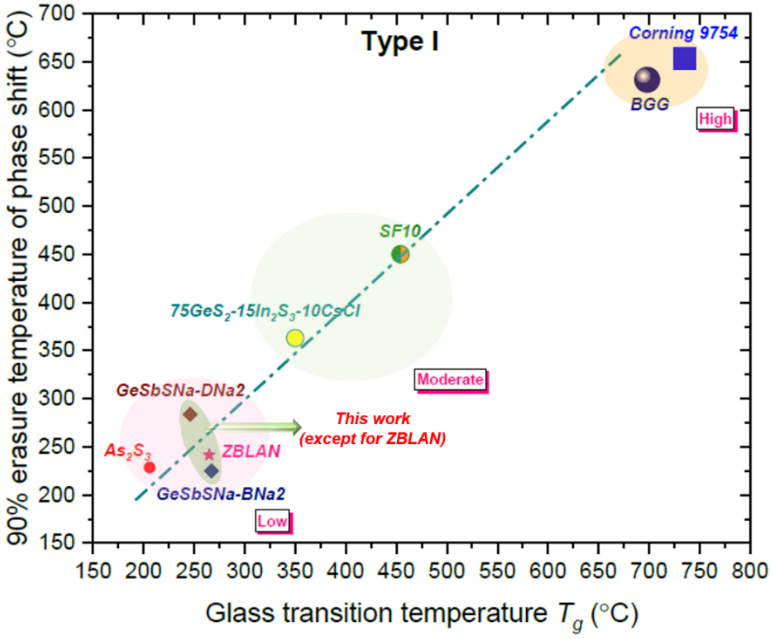

Fig. 6. Thermal stability of fs laser-induced Type I modifications in GeSbSNa glasses, expressed as the temperature at which 90% of the phase shift (the normalized phase shift falls to 10% of its initial value, i.e. $\Delta\phi(T)/\Delta\phi_0$ (20°C)= 0.10, where $\Delta\phi(T)$ is the remaining phase shift and $\Delta\phi_0$ is the initial phase shift at room temperature) is erased, plotted versus glass transition temperature (T_g). Data are compared with various glass families (oxides, chalcogenides, fluorides). The dashed line illustrates the general trend correlating T_g with modification stability. GeSbSNa glasses exhibit moderate thermal robustness, balancing MIR transparency with practical thermal endurance.

Data obtained in the present study on GeSbSNa glasses (e.g., DNa2, BNa2) are compared with various MIR-compatible glasses, including As_2S_3, SF10, BGG, ZBLAN, and commercial oxide glasses like Corning 9754. A general trend is observed: glasses with higher T_g exhibit greater thermal endurance of the laser-written modifications, following a quasi-linear relationship marked by the dashed trend line. This is consistent with previous reports on the nature of Type I modifications, which are known to be thermally erasable and structurally linked to defect generation and glass densification.

The GeSbSNa samples investigated in this work fall into the low to moderate thermal stability category, with erasure temperatures ranging from ~230 to ~290 °C, depending on composition. While these values are lower than those of oxide glasses (e.g., BGG or Corning 9754, which exceed 600 °C), they remain notably higher than those observed in classic chalcogenide systems like As_2S_3. This places GeSbSNa glasses in a favorable position for applications requiring a balance between MIR transparency and moderate thermal robustness.

Interestingly, the GeSbSNa-DNa2 glass shows improved thermal resistance compared to GeSbSNa-BNa2, which may be attributed to its higher sulfur content from 67 to 72 at.%. Elevated sulfur content has been associated with the formation of thermally stable S_8 rings, which dominate the glass structure at elevated temperatures and have been reported as the most abundant

Optics EXPRESS

species [32]. In contrast, ZBLAN glass—although widely used for fs inscription—deviates from the trend, likely due to its fluoride-based composition and poor thermal resilience.

Overall, while GeSbSNa glasses fall into the low-to-moderate thermal stability category compared to robust oxide systems, they offer a promising trade-off between a wide MIR transparency and laser-inscription photosensitivity. These results highlight the role of compositional tuning in controlling the balance between photosensitivity and thermal stability.

As is well established, the phase shift or RIC observed in fs laser-irradiated glasses originates from structural rearrangements, such as local volume changes, elemental migration, or reorganization of bonding configurations [14]. To investigate these modifications, Fig. 7 presents the normalized Raman spectra acquired from both the center of the fs-irradiated zone and the pristine region in GeSbSNa-ANa1 glass.

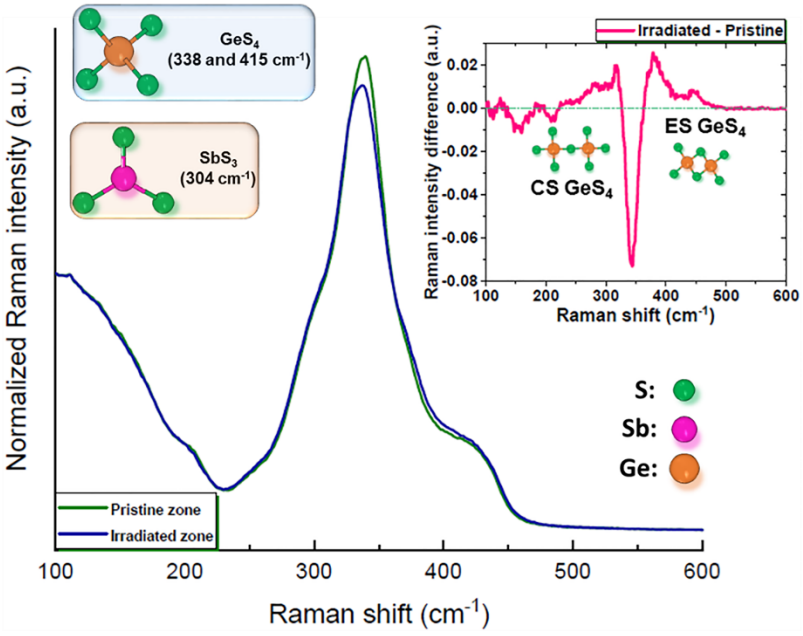

Fig. 7. Normalized Raman spectra acquired at the center (blue) and outside (green) of a fs laser-irradiated region in GeSbSNa-ANa1 glass. Main peaks are assigned to SbS_3 pyramids (~304 cm^{-1}) and GeS_4 tetrahedra (~338 and 415 cm^{-1}). The inset shows the differential spectrum (irradiated - pristine), revealing a laser-induced progressive transformation from CS to ES GeS_4 units, consistent with localized structural densification.

The spectra exhibit characteristic bands associated with the stretching vibrations of Ge–S bonds as well as Sb–S stretching modes from SbS_3 pyramidal units near 304 cm^{-1}. The peaks at 338 and 415 cm^{-1} can be attributed to corner-sharing (CS) GeS_4 configuration, meanwhile those at 377 and 444 cm^{-1} represent the edge-sharing (ES) arrangement of GeS_4 tetrahedra. These features are consistent with the known vibrational fingerprint of Ge–Sb–S chalcogenide networks. Here a subtle but distinct difference between the two spectra is observed, especially in the high-frequency region. To better resolve these changes, a difference spectrum (irradiated - pristine) is presented in the inset. This reveals a net increase in the vibrational features associated with ES slightly at the expense of CS GeS_4 tetrahedra following laser exposure. This laser-induced increase in the relative contribution of ES GeS_4 units at the expense of CS ones is indicative of a local densification and tightening of the Ge–S network in the irradiated volume. Such a structural rearrangement leads to an increase in the average bond density and enhanced electronic

Optics EXPRESS

polarizability, which directly contributes to the observed positive RIC in the modified region. Moreover, the absence of new sharp Raman peaks or significant bandwidth narrowing confirms that the laser-induced modifications remain amorphous and do not involve crystallization or phase separation under the present writing conditions. This supports the interpretation of Type I modifications in GeSbSNa glasses as densification-driven, point-defect-like changes rather than crystallization-induced refractive index variations.

This interpretation is further supported by the relative growth of the ES-related Raman modes in the 370–480 cm^{-1} range and the concomitant reduction of CS-related features near 338 cm^{-1}. Simultaneously, the reduction (after fs irradiation) of CS modes near 338 cm^{-1} may reflect subtle reorganization or clustering of GeS_4 units, potentially facilitating refractive index increases via enhanced polarizability. No significant shift is observed in the SbS_3 mode, indicating that the antimony coordination remains relatively stable under the fs laser conditions used. This implies that the structural response to laser irradiation is primarily driven by the germanium-sulfur sub-network, which governs both the short-range order and the optical properties. These findings support the hypothesis that Type I modifications in GeSbSNa glasses are accompanied by localized rearrangement of the network structure—particularly involving GeS_4 units—i.e., densification of the glass [6,22] rather than bond breaking or crystallization, consistent with the amorphous nature of the modifications.

4. Conclusions

This work demonstrated the remarkable tunability of refractive index and structural properties in sodium-doped GeSbS (GeSbSNa) chalcogenide glasses under fs laser irradiation. By varying sodium content and S/Ge ratio, we have identified key compositional parameters that govern photosensitivity, refractive index contrast (Δn up to 0.05), and thermal endurance of the laser-written features. Quantitative phase microscopy and Raman spectroscopy revealed that the observed modifications arise from localized densification and rearrangement of GeS_4 tetrahedra, while causing minimal disruption to the glass matrix. Importantly, the moderate thermal stability (erasure temperatures up to ~290 °C) places GeSbSNa glasses in a practical use position among MIR-transparent materials. These findings indicate that GeSbSNa glasses possess a combination of photosensitivity and thermal response that is compatible with 3D MIR photonic integration. While no MIR devices are fabricated in this work, the measured index contrasts and thermal erasure behavior are directly relevant for the design of future components such as lab-on-a-chip spectroscopy platforms, nonlinear MIR optics, or thermally stable waveguide structures.

Funding. National Natural Science Foundation of China (62505148); Zhejiang Provincial Natural Science Foundation of China (ZCLMS26F0502);China Postdoctoral Science Foundation (GZC20250572); National Key Research and Development Program of China (2021YFB2802000); Agence Nationale de la Recherche (ANR-18-CE08-0004-01); REFRACTEMP project (ANR-22-CE08-0001-01); China Scholarship Council (202206890050).

Disclosures. The authors declare that they have no known competing financial interests or personal relationships that could have appeared to influence the work reported in this paper.

Data availability. Data will be made available upon reasonable request.

References

1. Y. Wang, L. Zhong, K. Y. Lau, *et al.*, "Precise mode control of laser-written waveguides for broadband, low-dispersion 3D integrated optics," Light: Sci. Appl. **13**(1), 130–1195 (2024).
2. H. Yao, Q. Xie, M. Cavillon, *et al.*, "Materials roadmap for inscription of nanogratings inside transparent dielectrics using ultrafast lasers," Prog. Mater. Sci. **142**, 101226 (2024).
3. H. Yao, D. Pugliese, M. Lancry, *et al.*, "Ultrafast laser direct writing nanogratings and their engineering in transparent materials," Laser Photonics Rev. **18**(9), 2300891 (2024).
4. E. N. Glezer and E. Mazur, "Ultrafast-laser driven micro-explosions in transparent materials," Appl. Phys. Lett. **71**(7), 882–884 (1997).
5. H. Yao, R. Zaiter, M. Cavillon, *et al.*, "Photosensitivity of barium germano–gallate glasses under femtosecond laser direct writing for mid–IR applications," Ceram. Int. **47**(24), 34235–34241 (2021).

Optics EXPRESS

6. M. Lancry and B. Poumellec, "UV laser processing and multiphoton absorption processes in optical telecommunication fiber materials," Phys. Rep. **523**(4), 207–229 (2013).
7. Y. Zou, S. Chakravarty, C.-J. Chung, *et al.*, "Mid-infrared silicon photonic waveguides and devices [Invited]," Photonics Res. **6**(4), 254–276 (2018).
8. J. Tian, H. Yao, M. Cavillon, *et al.*, "A comparison between nanogratings-based and stress-engineered waveplates written by femtosecond laser in silica," Micromachines **11**(2), 131 (2020).
9. D. Tan, K. N. Sharafudeen, Y. Yue, *et al.*, "Femtosecond laser induced phenomena in transparent solid materials: Fundamentals and applications," Prog. Mater. Sci. **76**, 154–228 (2016).
10. Y. Gao and L. Cao, "Iterative projection meets sparsity regularization: towards practical single-shot quantitative phase imaging with in-line holography," Light Adv. Manuf. **4**(1), 1–53 (2023).
11. Y. Lei, G. Shayeganrad, H. Wang, *et al.*, "Efficient ultrafast laser writing with elliptical polarization," Light: Sci. Appl. **12**(1), 74 (2023).
12. J. Lapointe, Y. Ledemi, S. Loranger, *et al.*, "Fabrication of ultrafast laser written low-loss waveguides in flexible As_2S_3 chalcogenide glass tape," Opt. Lett. **41**(2), 203–206 (2016).
13. B. McMillen, B. Zhang, K. P. Chen, *et al.*, "Ultrafast laser fabrication of low-loss waveguides in chalcogenide glass with 0.65 dB/cm loss," Opt. Lett. **37**(9), 1418–1420 (2012).
14. T. T. Fernandez, L. Xu, S. Gross, *et al.*, "Physical mechanisms of femtosecond laser induced refractive index change in direct-written mid-infrared fiber Bragg gratings," APL Photonics **9**(11), 110802 (2024).
15. I. Pethes, V. Nazabal, J. Ari, *et al.*, "Atomic level structure of Ge-Sb-S glasses: Chemical short range order and long Sb-S bonds," J. Alloys Compd. **774**, 1009–1016 (2019).
16. B. Zhang, P. Zeng, Z. Yang, *et al.*, "On-chip chalcogenide microresonators with low-threshold parametric oscillation," Photonics Res. **9**(7), 1272–1279 (2021).
17. D. Xia, Z. Yang, P. Zeng, *et al.*, "Integrated chalcogenide photonics for microresonator soliton combs," Laser Photonics Rev. **17**(3), 2200219 (2023).
18. B. Morrison, A. Casas-Bedoya, G. Ren, *et al.*, "Compact Brillouin devices through hybrid integration on silicon," Optica **4**(8), 847–854 (2017).
19. R. Alvarado, L. Karam, R. Dahmani, *et al.*, "Patterning of the surface electrical potential on chalcogenide glasses by a thermoelectrical imprinting process," J. Phys. Chem. C **124**(42), 23150–23157 (2020).
20. M. David, D. Disnan, E. Arigliani, *et al.*, "Advanced mid-infrared plasmonic waveguides for on-chip integrated photonics," Photonics Res. **11**(10), 1694–1702 (2023).
21. C. R. Petersen, U. Møller, I. Kubat, *et al.*, "Mid-infrared supercontinuum covering the 1.4–13.3 µm molecular fingerprint region using ultra-high NA chalcogenide step-index fibre," Nat. Photonics **8**(11), 830–834 (2014).
22. M. Lancry, B. Poumellec, A. Chahid-Erraji, *et al.*, "Dependence of the femtosecond laser refractive index change thresholds on the chemical composition of doped-silica glasses," Opt. Mater. Express **1**(4), 711–723 (2011).
23. H. Yao, Q. Xie, M. Cavillon, *et al.*, "Volume nanogratings inscribed by ultrafast IR laser in alumino-borosilicate glasses," Opt. Express **31**(10), 15449–15460 (2023).
24. T. T. Fernandez, S. Gross, K. Privat, *et al.*, "Designer glasses—future of photonic device platforms," Adv. Funct. Mater. **32**(3), 2103103 (2022).
25. G. N. Greaves, "EXAFS and the structure of glass," J. Non-Cryst. Solids **71**(1-3), 203–217 (1985).
26. A. Lepicard, F. Bondu, M. Kang, *et al.*, "Long-lived monolithic micro-optics for multispectral GRIN applications," Sci. Rep. **8**(1), 7388 (2018).
27. G. Yang, Y. Liu, H. Liang, *et al.*, "Ultralow dispersion and broadband gradient refractive index microlens arrays imprinted in chalcohalide glass by microthermal poling," Ceram. Int. **50**(5), 7506–7513 (2024).
28. G. Yang, D. Zhou, M. Zhang, *et al.*, "The impact of anodic mesh density and halogen anions on the optical characteristics of gradient refractive index microlens arrays fabricated in chalcohalide glass via microthermal poling," Ceram. Int. **50**(22), 45610–45621 (2024).
29. R. Taylor, C. Hnatovsky, and E. Simova, "Applications of femtosecond laser induced self-organized planar nanocracks inside fused silica glass," Laser Photonics Rev. **2**(1-2), 26–46 (2008).
30. B. Poumellec, M. Lancry, A. Chahid-Erraji, *et al.*, "Modification thresholds in femtosecond laser processing of pure silica: review of dependencies on laser parameters [Invited]," Opt. Mater. Express **1**(4), 766–782 (2011).
31. C. D'Amico, C. Caillaud, P. K. Velpula, *et al.*, "Ultrafast laser-induced refractive index changes in $Ge_{15}As_{15}S_{70}$ chalcogenide glass," Opt. Mater. Express **6**(6), 1914–1928 (2016).
32. S. Susarla, T. Tsafack, P. S. Owuor, *et al.*, "High-K dielectric sulfur-selenium alloys," Sci. Adv. **5**(5), eaau9785 (2019).
33. G. Torun, A. Yadav, K. A. Richardson, *et al.*, "Ultrafast laser direct-writing of self-organized microstructures in Ge-Sb-S chalcogenide glass," Front. Phys. **10**, 883319 (2022).
34. C. Li, K. Li, J. Liu, *et al.*, "Design of a confocal dispersion objective lens based on the GRIN lens," Opt. Express **30**(24), 44290–44299 (2022).